SSCL-545

SSCL-545

Superconducting Super Collider Laboratory

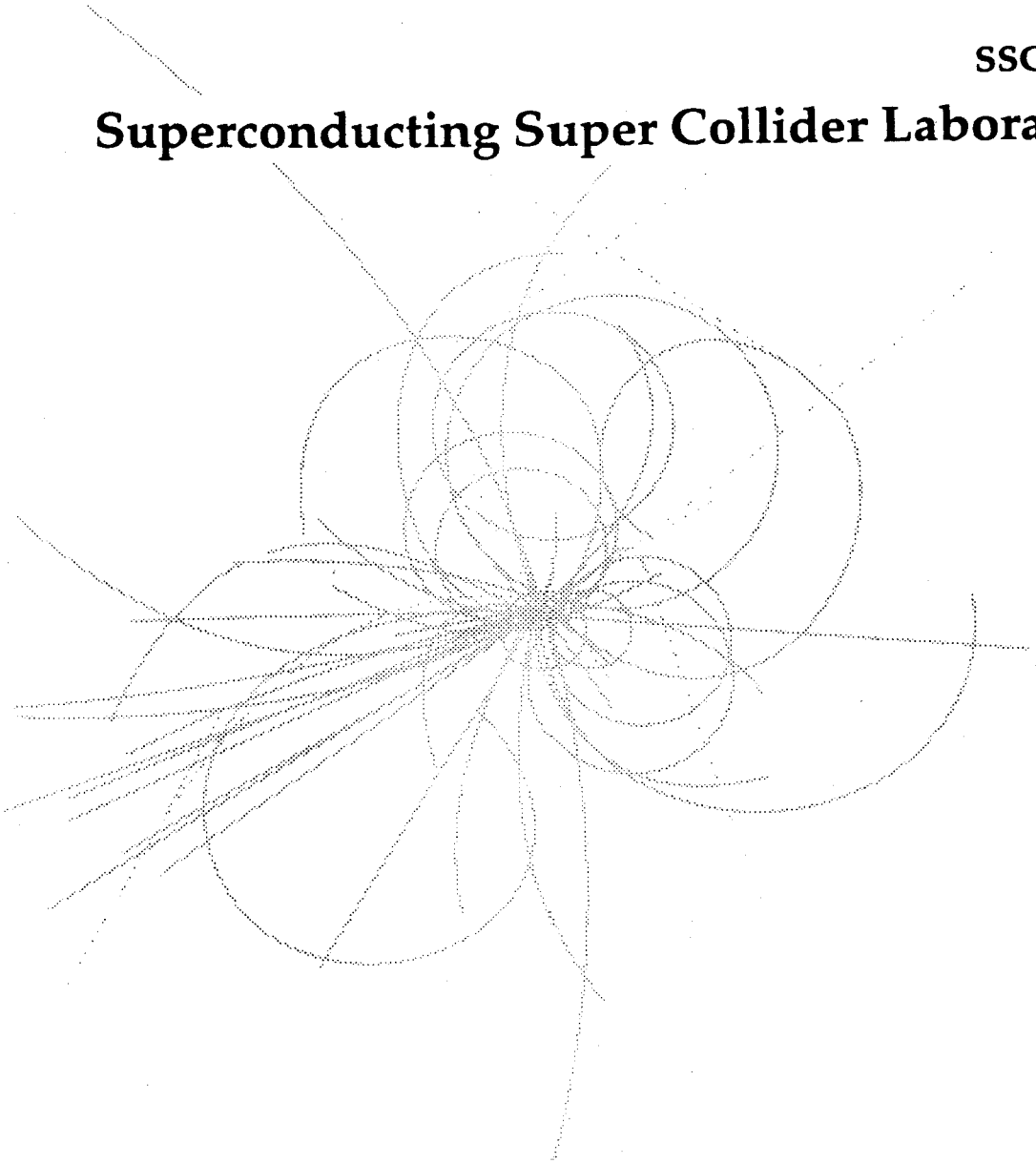

Ultrathin Crystal Scatterer for the SSC Beam Extraction System

A. Taratin, E. Tsyganov, M. Bavizhev,
A. Chao, H.-J. Shih, and T. Toohig

December 1991

SSCL-545

Ultrathin Crystal Scatterer for the SSC Beam Extraction System

A. Taratin and E. Tsyganov

Joint Institute for Nuclear Research
Dubna, USSR

M. Bavizhev

Institute of High Energy Physics
Serpukhov, USSR

A. Chao, H.-J. Shih, and T. Toohig

Superconducting Super Collider Laboratory*
2550 Beckleymeade Avenue
Dallas, TX 75237

December 1991

* Operated by the Universities Research Association, Inc., for the U.S. Department of Energy under Contract No. DE-AC35-89ER40486.

SSCL-545

Ultrathin Crystal Scatterer for the SSC Beam Extraction System

A. Taratin, E. Tsyganov, M. Bavizhev, A. Chao, H.-J. Shih, and T. Toohig

Abstract

It has been proposed to extract a 20 TeV beam from the SSC using a bent crystal to intercept halo particles which are then deflected by the channeling process into an extraction channel. There is concern that the halo particles induced by injecting noise into the rf system will strike the bent crystal deflector too close to the edge to be extracted. In this report we show that a thin straight crystal properly used in conjunction with the deflector can substantially widen the distribution of the hits across the deflector. This will allow less stringent requirements on the alignment and polishing of the deflector edge.

1.0 INTRODUCTION

There is a proposal[1] for doing B physics in a fixed target configuration by extracting a 20 TeV beam from the Superconducting Super Collider (SSC) with a bent crystal spectrometer. Since the SSC is a collider, this has to be done without interfering with collider experiments, i.e., the extraction rate should be at most comparable to the interaction rate of 10^8 protons per second at a high luminosity interaction point. The scheme of injecting filtered noise into the rf system has been considered and found effective in producing halo particles for extraction without perturbing the beam core.[2,3] Computer simulation[2] has shown a high extraction efficiency of nearly 90% at the SSC with a 3 cm long silicon crystal bent vertically by 100 μrad. However, it also revealed that most of the halo particles hit the bent crystal very close to its inner edge, within a distance of a few microns. Given these conditions, a septum width of 1 micron or smaller is needed which imposes stringent requirements on the orientation and polishing of the crystal edge. Moreover, assuming the halo particles hit the crystal within an area of $\sim 10\,\mu\text{m} \times 100\,\mu\text{m}$ at a rate of $10^8\,\text{sec}^{-1}$, this leads to a high particle flux of $10^{13}\,\text{cm}^{-2}\text{sec}^{-1}$, and thus possible severe radiation damage to the crystal.

In this paper it is shown by computer simulation that the distribution of the hits across the deflector (the bent crystal) can be significantly broadened if an ultrathin straight crystal is used to scatter the halo particles horizontally before they hit the deflector. How a thin straight crystal works to broaden the hit distribution and its advantages are explained in Section 2. Results from the computer simulation on multi-turn extraction with a double crystal system are presented in Section 3. A summary of study is then given in Section 4.

2.0 CRYSTAL SCATTERER

The motion of a planar channeled particle in a straight crystal is oscillatory and the transverse energy $E_x = (pv/2)x'^2 + U(x)$ is conserved. Here x is the distance from an atomic plane, p and v are the momentum and velocity of the particle, $U(x)$ is the planar continuum potential of the crystal and $x' = dx/dz$ is the angle relative to the channel direction z. The angle x' is maximal when the particle crosses the channel centerline. In the case that the particle enters the crystal parallel to the atomic planes, this maximal angle ψ is realized after it undergoes a quarter of one oscillation, and is given by $(pv/2)\psi^2 = U(x_0)$ where x_0 is the entrance coordinate. However, the oscillation wavelength λ depends upon the particle transverse energy E_x. The general relationship between λ and E_x is given by

$$\lambda(E_x) = 4 \times \int_{x_{\min}(E_x)}^{d_p/2} \left[\frac{E^*}{E_x - U(x)}\right]^{1/2} dx, \tag{1}$$

where d_p is the interplanar distance, $x_{\min}$ is the distance of closest approach to the plane and $E^* = pv/2$. Figures 1a and 1b show the E_x dependence of a quarter of one oscillation wavelength λ for 20 TeV protons in (110) planar channels of silicon and tungsten crystals respectively. It is seen that for silicon the relative change in λ is only about 25% whereas for tungsten it is about 44%. This is because the potential $U(x)$ for silicon is closer to a harmonic one.

As a result of the E_x dependence of λ, particles entering a crystal of a certain thickness with $x' = 0$ and a uniform distribution in x will exit from the crystal with a spread in x', i.e., the beam is scattered by the crystal. The spread in x' can be as large as the critical channeling angle ϑ_c, which is given by $(pv/2)\vartheta_c^2 = U(x_c)$ where x_c is the critical distance for channeling. Since $U(x_c)$ is roughly proportional to Z where Z is the atomic number of the crystal, one can expect a larger spread in x' if the beam is scattered by a crystal of higher Z. For comparison, ϑ_c is 1.5 μrad for silicon and 3.6 μrad for tungsten with $x_c = u_1$ where u_1 is the rms amplitude of the thermal vibrations of crystal atoms. Figures 2a and 2b show the angular distributions of a 20 TeV proton beam after it passes through a thin crystal of silicon and tungsten, respectively. As expected, the rms angle of the scattered beam is larger for the tungsten scatterer. Figures 3a and 3b show the dependence of the rms angle of the scattered beam upon the thickness of the crystal scatterer. The maximal value of the rms scattering angle is observed at a thickness of about 100 microns for silicon and about 50 microns for tungsten. At these thicknesses, the rms scattering angle is maximal because they correspond to about a quarter of the average oscillation wavelength.

The broadening of the angular distribution of a beam by a crystal scatterer can be used in bent crystal extraction to increase the distribution width of the hits across the deflector. This is demonstrated by assuming that the halo particles, before striking the deflector, strike a crystal scatterer with the (110) planes perpendicular to the plane of the reference orbit. If the halo particles enter the scatterer almost parallel to the (110) planes, the maximum rms scattering angle $\vartheta_{\rm sc}$ in the horizontal direction at the exit is about 0.8 μrad for a silicon scatterer and about 1.7 μrad for a tungsten scatterer, as seen in Figures 3a and 3b. The corresponding increment in the amplitude X_m of the horizontal betatron oscillation is given by

$$\Delta X_m(\vartheta_{\rm sc}) = \left(X_m^2 + \beta_{\rm sc}^2 \vartheta_{\rm sc}^2\right)^{1/2} - X_m. \tag{2}$$

where $\beta_{\rm sc}$ is the horizontal beta function at the position of the scatterer. The maximum increment in X_m, which occurs when $X_m = 0$, is $\beta_{\rm sc}\vartheta_{\rm sc}$. In the simulation, $\beta_{\rm sc}$ is 360 meters, so the maximum increment in X_m is 300 microns for a silicon scatterer and 600 microns

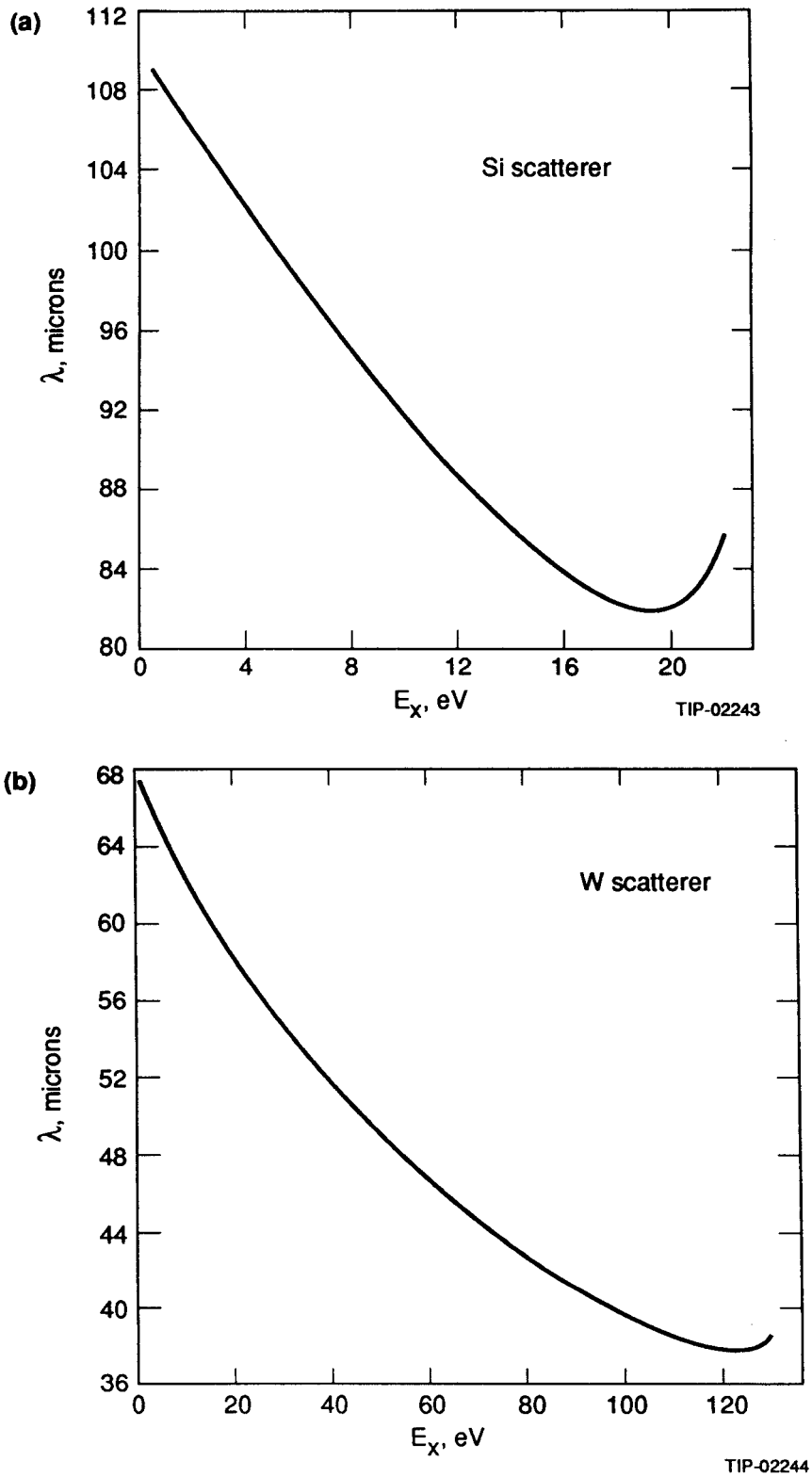

Figure 1. Dependence of a Quarter of One Oscillation Wavelength λ Upon Transverse Energy E_x for 20 TeV Protons in the (110) Planar Channels. (a) Silicon crystal. (b) Tungsten crystal.

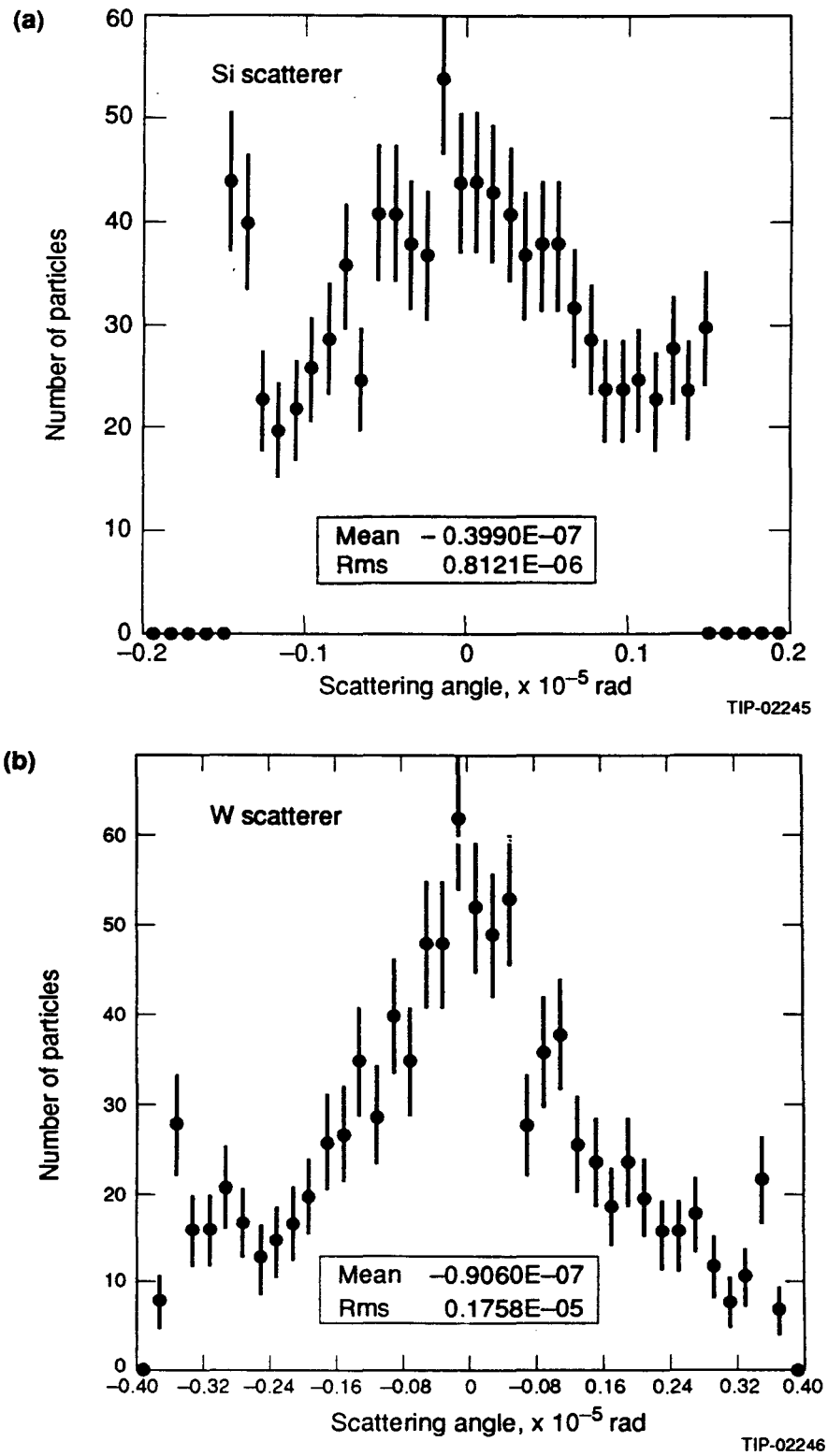

Figure 2. Angular Distributions of 20 TeV Protons Scattered by a Thin Straight Crystal. The protons enter the crystal parallel to the (110) planes. (a) A silicon crystal of thickness 80 microns. (b) A tungsten crystal of thickness 40 microns.

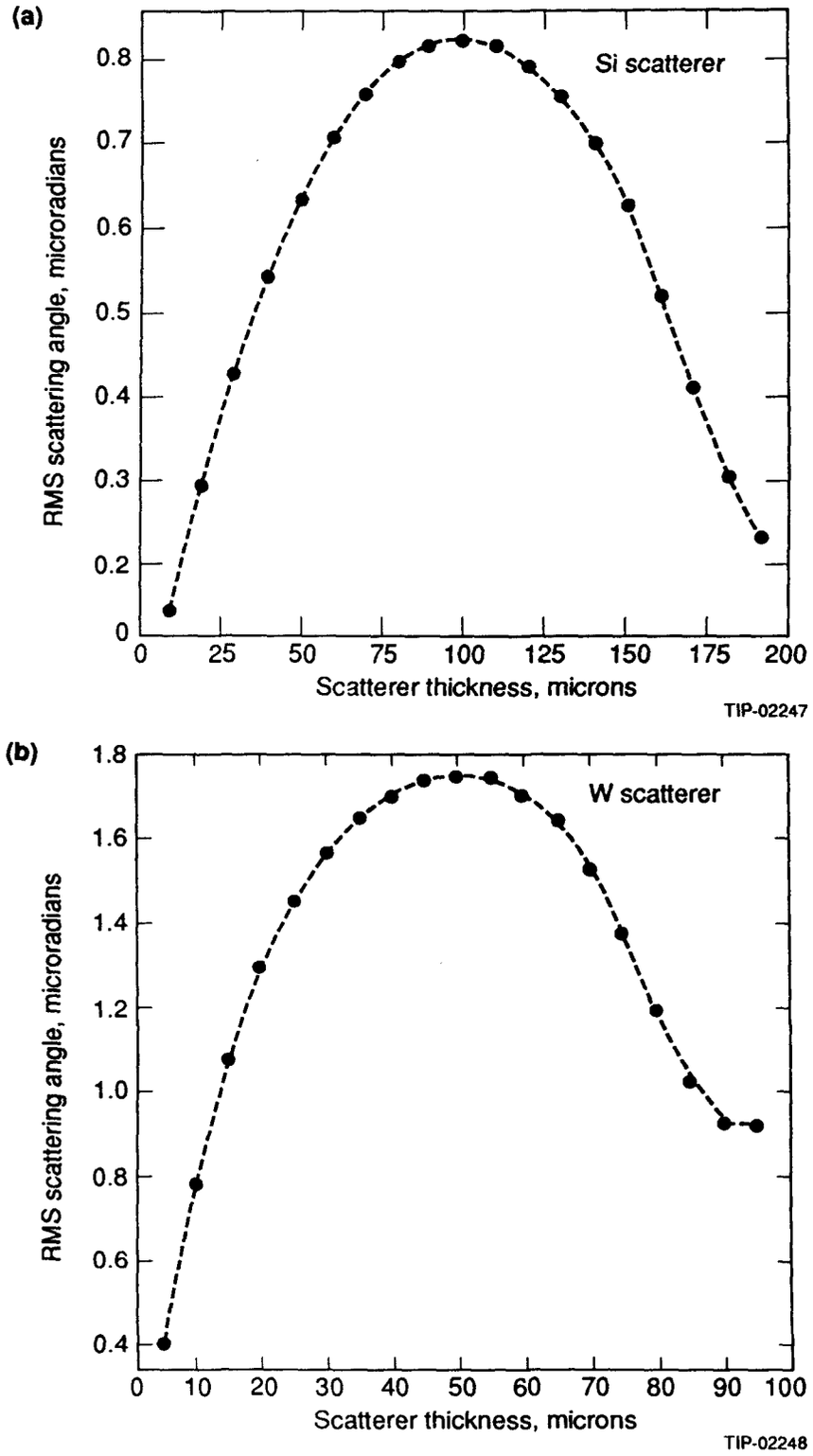

Figure 3. Dependence of the rms Scattering Angle of 20 TeV Protons Upon the Thickness of the Crystal Scatterer. The protons enter the scatterer parallel to the (110) planes. (a) A silicon scatterer. (b) A tungsten scatterer.

for a tungsten scatterer. This increase in the amplitude of the horizontal betatron motion then allows the halo particles after a few turns to intercept the deflector farther away from the design orbit thereby widening the distribution of the hits across the deflector.

The disturbance of the beam halo in the vertical direction by a thin crystal scatterer is negligible, because the multiple scattering angle $\vartheta_{\rm ms}$ at the length of the scatterer is very small, $\vartheta_{\rm ms} \approx 0.01\,\mu$rad. Because of this, the extraction efficiency of the deflector which depends on the angular divergence in the vertical direction of the beam is not affected. This is an important feature of a crystal scatterer. In case of an amorphous scatterer, $\vartheta_{\rm ms}$ in the vertical direction is greater and the extraction efficiency of the deflector will be reduced. In addition, the thin scatterer can endure more radiation damage than a longer crystal (e.g., the 3 cm long deflector) because even though the dechanneling length decreases significantly it is still much longer than the length of the scatterer so there will be little degradation in channeling efficiency.

3.0 BEAM EXTRACTION WITH A DOUBLE CRYSTAL SYSTEM

Two parameters associated with the scatterer need to be fixed as input to the simulation: its location in the Collider ring and its distance from the design orbit. Considering particles with a given Courant-Snyder invariant A, because of the injection of rf noise, their orbits in longitudinal phase space gradually diffuse toward the separatrix. They will begin to hit the crystal deflector if their relative momentum deviation $\Delta p/p$ is such that

$$x_{\rm bc} = A\sqrt{\beta_{\rm bc}} + \eta_{\rm bc}\frac{\Delta p}{p} \tag{3}$$

where $\beta_{\rm bc}$ and $\eta_{\rm bc}$ are the beta function and dispersion, respectively, at the position of the deflector and $x_{\rm bc}$ is the distance of the deflector inner edge from the design orbit. To make these particles pass through the scatterer before they hit the deflector, the distance of the scatterer inner edge $x_{\rm sc}$ from the design orbit should satisfy

$$\begin{aligned} x_{\rm sc} &< A\sqrt{\beta_{\rm sc}} + \eta_{\rm sc}\frac{\Delta p}{p} \\ &= A\sqrt{\beta_{\rm sc}} + \frac{\eta_{\rm sc}}{\eta_{\rm bc}}\left(x_{\rm bc} - A\sqrt{\beta_{\rm bc}}\right) \\ &= A\left(\sqrt{\beta_{\rm sc}} - \frac{\eta_{\rm sc}}{\eta_{\rm bc}}\sqrt{\beta_{\rm bc}}\right) + \frac{\eta_{\rm sc}}{\eta_{\rm bc}}x_{\rm bc} \end{aligned} \tag{4}$$

where $\eta_{\rm sc}$ is the dispersion at the position of the scatterer. Since the value of $x_{\rm sc}$ chosen to satisfy Eq. (4) is expected to be good for all particles, i.e., any value of A, the scatterer

should be located at such a position that

$$\sqrt{\frac{\beta_{sc}}{\beta_{bc}}} = \frac{\eta_{sc}}{\eta_{bc}}. \tag{5}$$

A natural choice is to place the scatterer at the position of the deflector. In this case $x_{sc} < x_{bc}$, i.e., the scatterer inner edge should be closer to the design orbit than the deflector inner edge. In the simulation, the scatterer was placed immediately behind the deflector in the beam direction, as shown in Figure 4, x_{sc} was fixed at 1 cm and x_{bc} was varied in order to obtain an optimized offset $d = x_{bc} - x_{sc}$ for the distribution of the hits across the deflector.

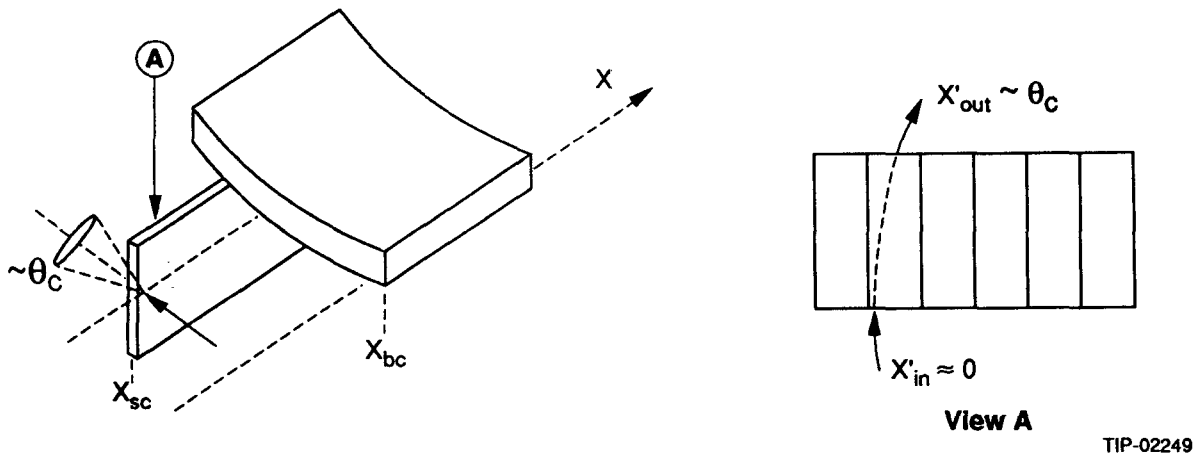

Figure 4. Proposed Extraction Scheme with an Ultrathin Crystal Scatterer. The deflector (a bent crystal) is immediately followed by the scatterer (a thin straight crystal) in the beam direction. The scatterer with a thickness of approximately a quarter of the average oscillation wavelength provides an angular kick x' of the order of ϑ_c, the channeling critical angle.

Computer simulation of the multi-turn SSC beam extraction with a bent crystal deflector plus an ultrathin crystal scatterer was conducted in the same manner as that presented in Reference 2. The particle trajectories in the crystal scatterer were calculated according to the same scheme as that in the crystal deflector. The optimal scatterer thickness determined from Section 2, 100 microns for silicon and 50 microns for tungsten, was used. The beam halo particles were again produced by injecting filtered noise into the rf system. The (110) planes of the scatterer were perpendicular to the plane of the SSC collider ring and tangential to the design orbit so that the angles of the particles striking the scatterer relative to the atomic planes were minimized. Two linear 6×6 transfer maps representing the two sections of the collider lattice between the double crystal system and the rf system were used to transport particles around the ring.

The broadening of the distribution of the hits across the deflector by a crystal scatterer was observed in the simulation. This is shown in Figures 5a and 5b for two offsets, 100 and 1000 microns. Without a scatterer, the average distance of the hits from the deflector inner edge, $\overline{\Delta x} = \overline{x - x_{\rm bc}}$, was about 20 microns, as seen in Reference 2. It was increased to about 140 microns with a silicon scatterer and about 400 microns with a tungsten scatterer for an offset of 100 microns. As explained in the last section, the reason for this broadening is that the halo particles enter the (110) planar channels of the scatterer at small angles $x' \ll \vartheta_c$, perform approximately a quarter of one oscillation during the passage, and exit at angles of the order of ϑ_c. As a result the halo particles obtain larger horizontal betatron oscillations and after a few turns can intercept the deflector at a greater distance from the design orbit.

Figures 6a and 6b show the average distance $\overline{\Delta x}$ of the hits from the deflector inner edge as a function of the offset between the deflector and scatterer d. $\overline{\Delta x}$ quickly rises over an increase of a few tens of microns in d. It reaches the maximum when d is about $50 \sim 100$ microns for a silicon scatterer and about $100 \sim 200$ microns for a tungsten scatterer. This increase is due to the fact that when the deflector is only slightly displaced from the scatterer, there are still particles that strike the deflector without passing through the scatterer, but as the deflector is moved farther away from the scatterer, there will be an increase in the number of halo particles that pass through the scatterer once before they strike the deflector. However, the extracted particles pass through the scatterer more than once when the offset is relatively large. The d dependence of the number of passages through the scatterer is illustrated in Figure 7a for a silicon scatterer and Figure 7b for a tungsten scatterer. As the number of passages increases, the average angle relative to the atomic planes of the scatterer increases (and so does the transverse energy), and more particles pass through it in quasi-channeling states. Thus, their average deflection angle by the scatterer, $\vartheta_{\rm sc}$, becomes smaller. In addition, the initial amplitude of their horizontal betatron oscillations, X_m, increases. The increment in the horizontal betatron amplitude, as can be seen from Eq. (2), decreases and the particles intercept the deflector closer to its inner edge. This is a contributing factor for the decrease in $\overline{\Delta x}$ when d is relatively large, as seen from Figures 6a and 6b. Another contributing factor is that, as d increases, the region near the deflector inner edge has more probability to accumulate the particles that strike the scatterer at different points. The distribution of hits across the deflector shown in Figures 5a and 5b for an offset of 1000 microns illustrates the peak reappearing near the deflector inner edge.

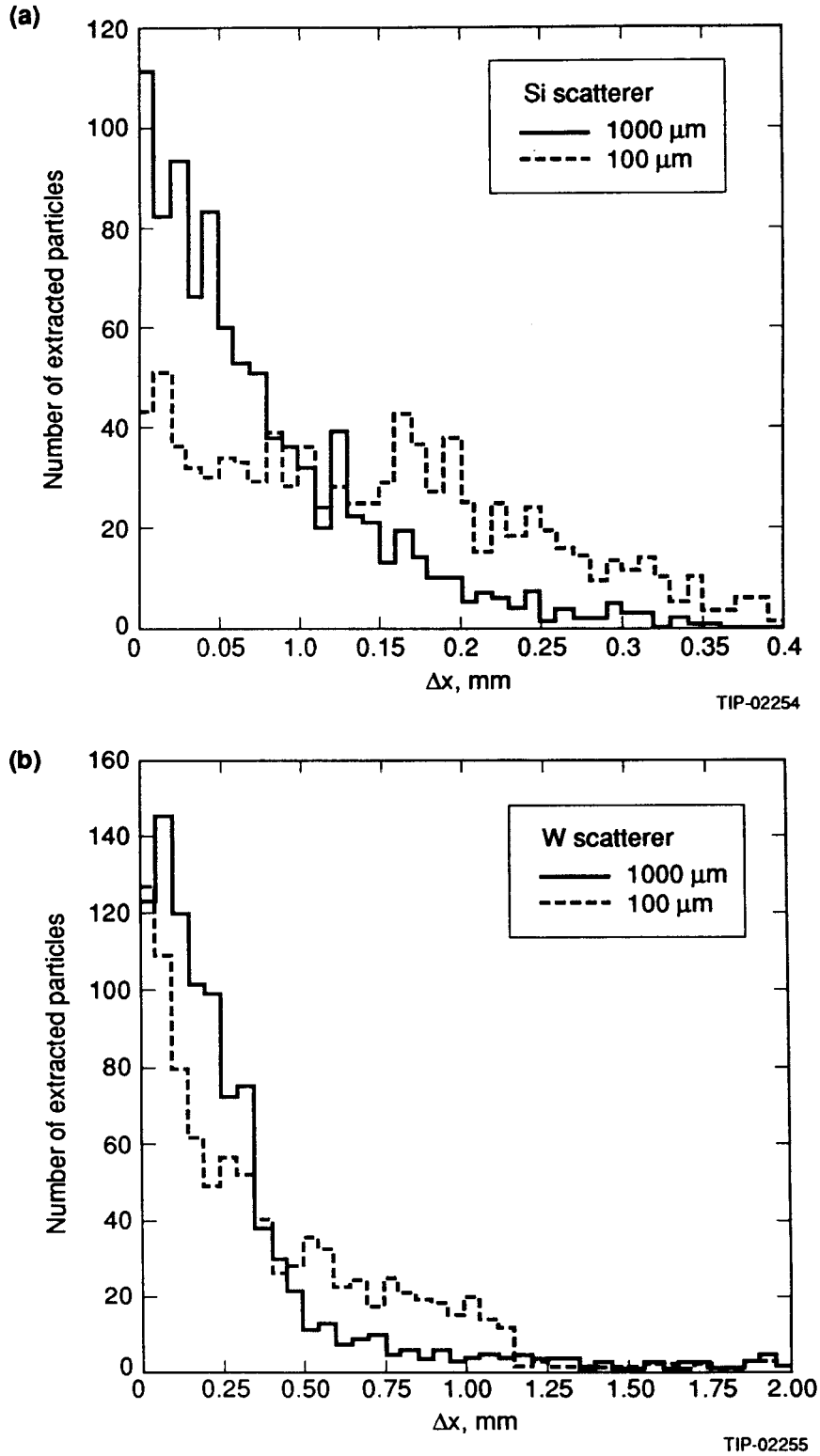

Figure 5. Distributions of Extracted Particles in the Distance of the Entry Point to the Deflector. (a) A silicon scatterer; solid curve: $d = 100$ microns, dashed curve: $d = 1000$ microns. (b) A tungsten scatterer; solid curve: $d = 100$ microns, dashed curve: $d = 1000$ microns. d is the offset between the deflector and scatterer.

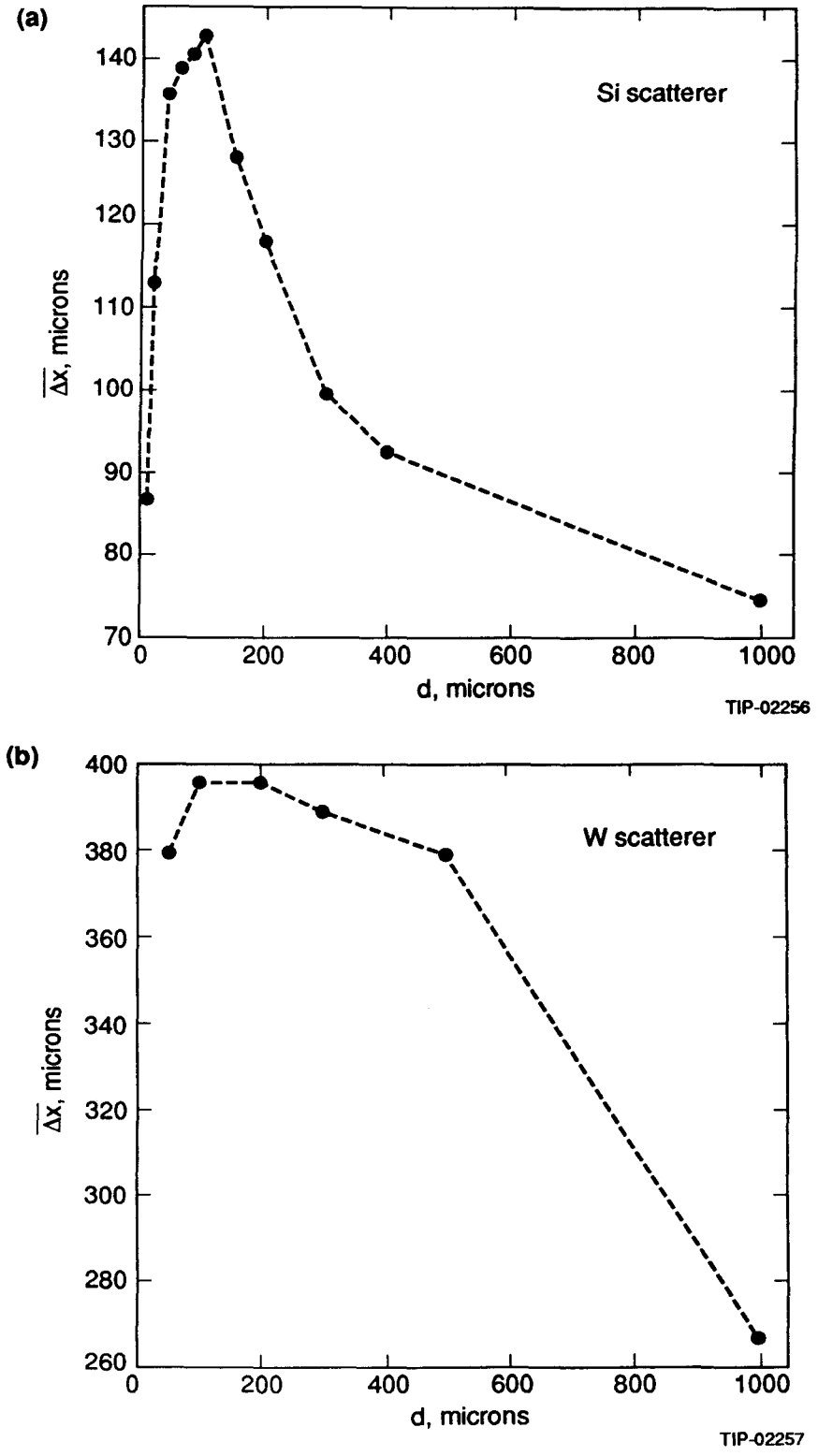

Figure 6. Average Distance of the Entry Point to the Deflector of Extracted Particles as a Function of the Offset Between the Deflector and Scatterer. (a) A silicon scatterer. (b) A tungsten scatterer.

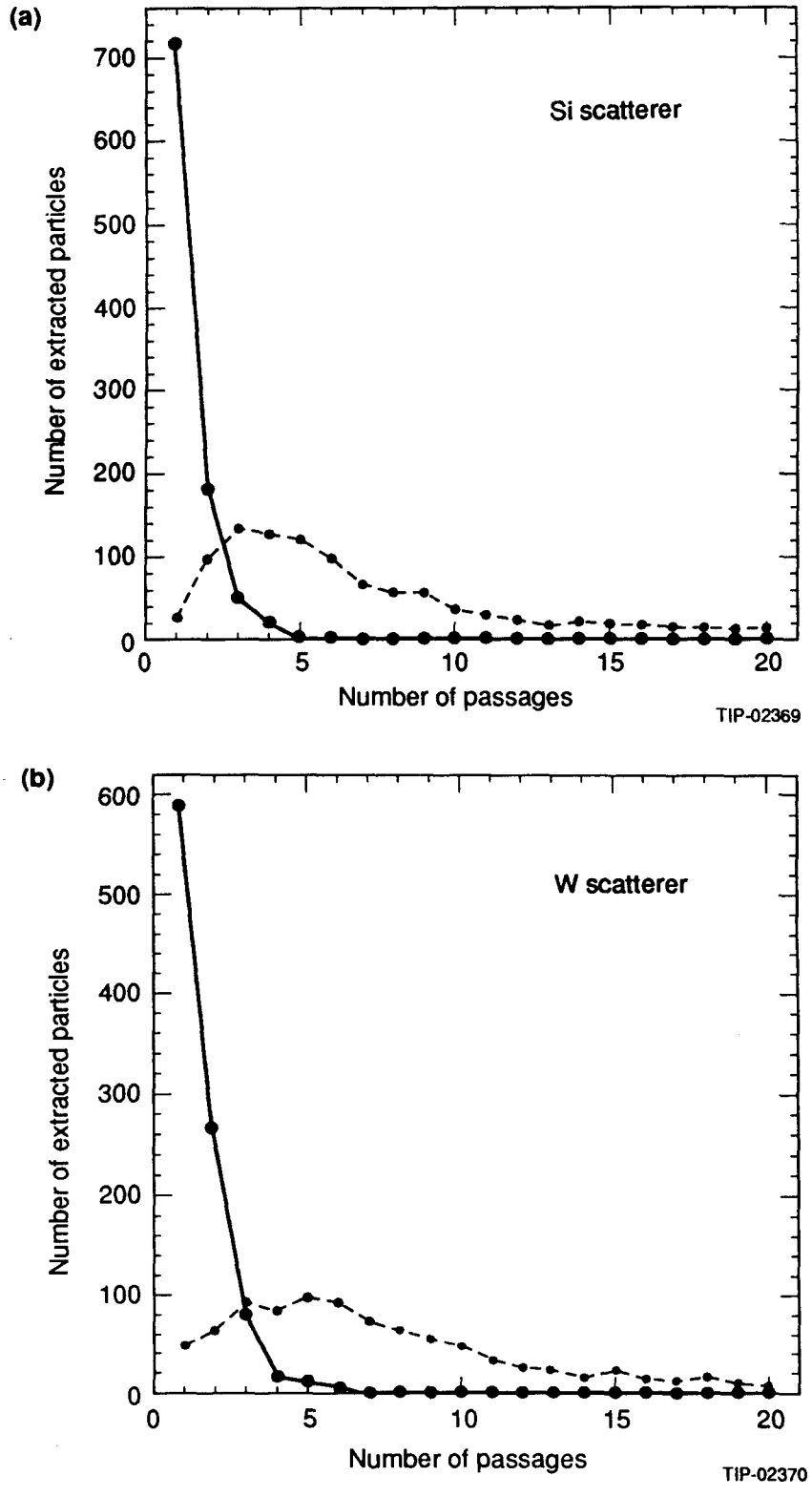

Figure 7. Distributions of Extracted Particles in the Number of Passages Through the Scatterer. (a) A silicon scatterer; solid curve: $d = 40$ microns, dashed curve: $d = 400$ microns. (b) A tungsten scatterer; solid curve: $d = 100$ microns, dashed curve: $d = 1000$ microns. d is the offset between the deflector and scatterer.

4.0 CONCLUSION

Using computer simulation, it has been demonstrated that an ultrathin crystal scatterer, used properly in conjunction with a bent crystal deflector, has the effect of broadening the distribution of the particle hits across the deflector. This effect has been investigated using the (110) planar channels of silicon and tungsten crystals as the scatterer. The optimum thickness of the scatterer was shown to be 100 microns for silicon and 50 microns for tungsten for 20 TeV protons incident on the scatterer parallel to the (110) planes. Using silicon and tungsten scatterers with the optimum thickness, it has been shown that the distribution of particle hits across the deflector is most broadened when the offset between the scatterer and deflector is in the range $50 \sim 100$ microns for a silicon scatterer and in the range $100 \sim 200$ microns for a tungsten scatterer. The maximum average distance of hits from the deflector inner edge is about 140 microns for a silicon scatterer and about 400 microns for a tungsten scatterer. In comparison, the average distance of hits is only about 20 microns when no scatterer is used.

ACKNOWLEDGEMENTS

The authors would like to thank D. Carrigan, Jr., B. Cox, J. Ellison, T. Murphy, B. Newberger, and S. Peggs for useful discussions.

REFERENCES

1. The SFT Collaboration, *An Expression of Interest in a Super Fixed Target Beauty Facility at the SSC*, EOI-14, submitted to the SSC PAC, 25 May 1990.

2. H.-J. Shih and A.M. Taratin, *Bent Crystal Extraction of the SSC Beam with RF Noise Induced Diffusion*, SSC Laboratory Report SSCL-389, March 1991.

3. J.A. Ellison, B.S. Newberger and H.-J. Shih, *Effect of rf Phase Noise on the SSC beam*, SSC Laboratory Report SSCL-432, May 1991, to be published in Proc. 14th Biennial Particle Accelerator Conference, San Francisco, CA, May 6–10, 1991.